Article

A multifunctional polymer combining the imidazole and zwitterion motifs as a biocompatible compact coating for Quantum Dots

Wentao Wang, Xin Ji, Anshika Kapur, Chengqi Zhang, and Hedi Mattoussi

J. Am. Chem. Soc., **Just Accepted Manuscript** • DOI: 10.1021/jacs.5b08915 • Publication Date (Web): 14 Oct 2015

A multifunctional polymer combining the imidazole and zwitterion motifs as a biocompatible compact coating for Quantum Dots

Wentao Wang, Xin Ji, Anshika Kapur, Chengqi Zhang, Hedi Mattoussi

Department of Chemistry and Biochemistry, Florida State University, 95 Chieftan Way, Tallahassee, Florida 32306, USA

Keywords: quantum dots, surface functionalization, imidazole, zwitterion, polymer ligand, multi-coordination, sensing and imaging.

Abstract

We introduce a set of multi-coordinating imidazole- and zwitterion-based ligands suited for surface-functionalizing quantum dots (QDs). The polymeric ligands are built using a one-step nucleophilic addition reaction between poly(isobutylene-*alt*-maleic anhydride) and distinct amine-containing functionalities. This has allowed us to introduce several imidazole anchoring groups along the chain, to tightly coordinate onto the QD surface, and a controllable number of zwitterion moieties for water solubilization. It has also permitted the introduction of reactive and biomolecular groups to allow for further conjugation and targeting. The QDs capped with these new ligands exhibit excellent long-term colloidal stability over a broad range of pH, to excess electrolyte, in cell growth media and in the presence of natural reducing agents such as glutathione. These QDs are also resistant to the oxidizing agent H_2O_2. More importantly, by using zwitterion moieties as the hydrophilic block, this polymer design provides QDs with thin coating and compact overall dimensions. These QDs are easily self-assembled with full size proteins expressed with a polyhistidine tag via metal-histidine coordination. Additionally, incorporation of amine groups allows covalent coupling of the QDs to the neurotransmitter dopamine. This has yielded redox active QD platforms that were used to track pH changes, sensing interactions with Fe ions and cysteine. Finally, we found that QDs cap exchanged with folic acid-functionalized ligands could effectively target cancer cells, where folate receptor-mediated endocytosis of QDs into living cells was time- and concentration-dependent.

Email: mattoussi@chem.fsu.edu

Introduction

Semiconductor nanocrystals (quantum dots, QDs) along with metal and metal-oxide nanoparticles possess unique size and/or composition-tunable physical and spectroscopic properties.[1-5] For instance, QDs such as ZnS-overcoated CdSe nanocrystals exhibit narrow emission with high quantum yield and remarkable photostability.[6-8] Additionally, because these nanocrystals are in a size range comparable to those of biomolecules, they are very attractive for use as imaging probes and as sensing and diagnostic tools.[9-20] Nonetheless, application of these materials in biology is still limited by constraints that include a rather large hydrodynamic size and limited colloidal stability.[21-26] The large size negatively affects their transport properties in biological media, such as cellular internalization, blood vasculature circulation lifetime and renal clearance.[21,22,25-27] Furthermore, several important *in vivo* studies, such as the fluorescence tracking of protein dynamics and detection of individual binding events, require the use of very small reagent concentrations.[28] However, achieving robust colloidal stability of hydrophilic QDs at nanomolar concentrations and under ambient conditions is still challenging.[23,24] These properties are primarily dependent on the nature of the capping ligands and the surface coating strategy used to functionalize the nanocrystals.

Water solubilization of high quality QDs and other nanocrystals, prepared using high temperature growth routes, has been achieved via either cap exchange with thiol-based metal-coordinating ligands or encapsulation within amphiphilic block copolymers and phospholipid micelles.[9,29-36] However, both approaches have faced inherent limitations. For example, under room temperature and light exposure conditions, thiol-based ligands tend to oxidize with time, which can cause ligand desorption from the QD surface and result in aggregation; this is particularly important at very low reagent concentrations.[23,37-39] In addition, thiol coordination has been reported to weaken the QD fluorescence.[40] Conversely, the encapsulation strategy produces nanoparticles with limited stability at low concentrations and it also tends to significantly increase the hydrodynamic radius of the QDs.[34,41]

Recently, several strategies have been explored to alleviate the above issues. To minimize the hydrodynamic size of the QDs without sacrificing aqueous solubility, a series of dihydrolipoic acid (DHLA)-based ligands appended with zwitterion groups have been developed as an alternative to poly(ethylene glycol) (PEG).[24,42-47] Due to their small volume, ligands based on the zwitterion motif yield nanocrystals with compact size. Additionally, imidazole-based

ligands have been proposed by a few groups as an alternative to thiols, because they are not affected by oxidation and tend to maintain high QD photoluminescence (PL).[23,25,48,49]

In this study, a set of polyimidazole-based zwitterionic ligands have been developed to promote the phase transfer of hydrophobic QDs to aqueous media. This ligand design combines the benefits of the small size zwitterion with imidazole coordination. The ligand synthesis relies on the one-step nucleophilic addition reaction of distinct amine-containing functionalities with poly(isobutylene-*alt*-maleic anhydride), PIMA. The resulting modular ligands have: multi-imidazoles for metal-coordination on the QD, several zwitterion moieties for water solubilization and reactive groups for bioconjugation, as shown in Figure 1. In particular, this synthetic route allows the insertion of target biomolecules in-situ during ligand synthesis, thus integrating hydrophilic modification and bioconjugation of the QDs in one step (e.g., scheme 2 in Figure 1).

Functionalizing the QDs with these ligands produces dispersions that are highly fluorescent and exhibit long-term stability over a broad range of conditions, including in growth media, in the presence of oxidizing agents, and storage at nanomolar concentrations under room temperature and light exposure conditions. Substituting PEG with zwitterion moieties produces QDs that are compact and easily conjugated with His-tagged proteins.[50-54] Additionally, covalent attachment of the neurotransmitter dopamine to QDs capped with amine-modified polymer ligands, provides a platform that can be used to sense pH changes, iron ion and cysteine amino acid via charge transfer interactions. Finally, we show that folic acid-modified ligands can promote the delivery of large amounts of QDs into living cells through folate receptor-mediated endocytosis.

Results and Discussion

Ligand Design. The present ligand design builds on previous ideas where the highly efficient and specific nucleophilic addition reaction of maleic anhydride towards amine-presenting molecules/moieties has been exploited.[31,35,39,55] For example, we have applied this route, starting with poly(isobutylene-*alt*-maleic anhydride), PIMA, to prepare a few poly(ethylene glycol)-modified, metal-coordinating ligands for surface functionalization of QDs or Fe_3O_4 nanoparticles.[39,55] Here, we extend those rationales to prepare a set of hydrophilic, multi-coordinating polymer ligands based on the zwitterion motif. The ability to carry out synthesis without the need for coupling reagents or excess precursors eliminates constraints associated with compound purification, due to limited solubility of the zwitterion groups in organic solvents. In addition, this one-step reaction route is easy to implement, compared to other polymer ligand designs, which tend to require multistep synthesis with attendant purification requirements.[23]

Figure 1 summarizes the general schemes employed to prepare two sets of imidazole- and zwitterion-modified polymers: one set is made of bio-reactive ligands while the second is made of PIMA simultaneously coupled to zwitterion groups and biological receptors. 1) The bio-reactive ligand refers to the polymer presenting zwitterion and reactive groups (such as carboxy, amine, and azide) along its backbone; the latter could be used for further coupling to target biomolecules. This set includes His-PIMA-ZW, made by reacting PIMA with a mixture of histamine (50%) and amino-zwitterion (50%). It is expected to introduce about 20 imidazole anchors and 20 zwitterion moieties, while freeing ~40 reactive carboxylic groups per PIMA chain. These carboxylic groups can be used for conjugating the polymer-coated QDs to biomolecules, such as transferrin via EDC/NHS chemistry. Another representative ligand is made from a stoichiometric mixture of histamine, amino-zwitterion and reactive groups, His-PIMA-ZW/R (R = amine, azide, or biotin). This can be achieved by replacing a fraction of the amino-zwitterion moieties with H_2N-PEG-R during the addition reaction. We have, for example, prepared His-PIMA-ZW/NH_2 ligands where the PIMA was modified with 10% H_2N-PEG-NH_2 together with 40% amino-zwitterion and 50% histamine. 2) The bio-functionalized ligands are prepared by introducing amine-presenting biomolecules, along with histamine and amino-zwitterion onto the PIMA chain during the nucleophilic addition reaction. We have synthesized a ligand His-PIMA-ZW/FA, modified with 10% folic acid (along with 50% histamine and 40% amino-zwitterion), as a coating with potential cancer cell targeting capacity. Indeed QDs

functionalized with His-PIMA-ZW/FA have been employed to target and deliver large amounts of QDs into living cells (see below). We should note that this scheme could, in principle, be used to introduce an array of amine-rich biomolecules into the polymer ligand, such as amine-terminated peptides or proteins.

Ligand Exchange and Characterization of the Hydrophilic QDs. Ligand exchange was performed following the protocols described in reference,[56] but with a few slight modifications. To circumvent the limited solubility of zwitterion groups in commonly used organic solvents, the ligands (e.g., His-PIMA-ZW) were dissolved in small amounts of DMSO prior to mixing with the hydrophobic QDs dispersed in chloroform. The mixture was left stirring at room temperature overnight. The displaced native ligands (TOP/TOPO and such) were then removed by two rounds of precipitation using a mixture of hexane and acetone, followed by centrifugation. After gentle drying, the QD pellet was readily dispersed in buffer. Further purification of the QD dispersion was carried out using two rounds of concentration/dilution with DI water using a centrifugal filtration device, yielding a clear and homogeneous colloidal suspension of nanocrystals. The hydrophilic QDs ligated with His-PIMA-ZW were characterized by: optical spectroscopy, ^{1}H and ^{31}P NMR spectroscopy, diffusion-ordered spectroscopy and dynamic light scattering. The ^{1}H NMR data were further exploited to extract an estimate of the ligand density on the QD surfaces.

1) Optical characterization. Figure 2A shows the absorption and emission spectra of a representative set of green-emitting QDs (emission peak at 556 nm) before and after ligand exchange with His-PIMA-ZW. The spectra of hydrophilic QDs exhibit identical profiles to those collected for the starting materials (TOP/TOPO-capped), indicating that the integrity of the nanocrystals following phase transfer was maintained. The quantum yield (QY) of the QDs after ligand exchange was evaluated by comparing the PL of water dispersible QDs to that measured from the hydrophobic ones dispersed in hexane. The relative PL intensity of the aqueous QDs with respect to the hydrophobic dispersions was ~90% (see Figure 2B). This rather high PL of the hydrophilic QDs derives from the benefits of imidazole coordination onto the QD surfaces;[39] it confirms and complements prior observations where conjugation of polyhistidine-tagged proteins onto DHLA-capped QDs produced a sizable enhancement in the PL signal.[51,52]

Additional data on the optical characterization of other QD samples, ligated with His-PIMA-ZW and His-PIMA-ZW/FA, are provided in the Supporting Information (Figure S2).

2) NMR characterization. The ^{1}H NMR spectrum in Figure 2C, collected from His-PIMA-ZW-QDs, shows two distinct peaks at 7.03 and 7.17 ppm characteristic of the two protons in the imidazole ring; these peaks are slightly shifted and have lower intensity than those measured for the pure ligand, due to a change in environment following coordination onto the QD surfaces.[39] The pronounced resonance at 3.00 ppm corresponds to the methyl groups of the zwitterion moieties, while the smaller peaks at 2.10, 2.85, 3.27 and 3.35 ppm are ascribed to the protons in the CH_2 of the zwitterion and imidazole moieties (see Figure 2C). The broad peak at ~0.89 ppm is ascribed to the methyl protons in the PIMA chain. Similarly, the ^{31}P NMR spectrum collected from a dispersion of His-PIMA-ZW-QDs shows that the two sharp peaks at ~ -30 ppm and ~50 ppm and the weak peak at ~37 ppm, measured for the hydrophobic QDs and respectively attributed to trioctylphosphine (TOP), trioctylphosphine oxide (TOPO) and hexylphosphonic acid (HPA), have disappeared following ligand exchange (see Supporting Information, Figure S3). These data indicate that cap exchange with His-PIMA-ZW is highly efficient and is driven by the coordination of the imidazole groups onto the QDs. Additional ^{1}H NMR data from QDs ligated with His-PIMA-ZW/FA are shown in the Supporting Information (Figure S4).

3) Diffusion-ordered spectroscopy and dynamic light scattering. Diffusion-ordered NMR spectroscopy (simply DOSY) is a versatile, non-destructive technique that can resolve the diffusion coefficient, D, of sub-nanometer objects in solution, which makes it more suitable than dynamic light scattering for characterizing rather small nanoparticles. It exploits the time-dependent signature of NMR active atoms (e.g., ^{1}H, ^{13}C, or ^{31}P) in a molecule of interest dispersed in a deuterated solution.[57] When applied to colloidal nanocrystals, DOSY provides a measure of the diffusion coefficients of ligands (associated with the observed resonances); thereby it permits the assignment of spectral features in the measured ^{1}H NMR spectrum to diffusing species that are either bound on the nanocrystals or free in the medium. For QDs ligated with His-PIMA-ZW, the various resonances in its ^{1}H NMR spectrum can be ascribed to two distinct diffusion coefficients (see Figure 2D). The faster diffusion ($D = 1.78 \times 10^{-9}$ m^2/s) is attributed to solubilized water molecules in the sample, while the smaller value ($D = 4.16 \times 10^{-11}$ m^2/s) associated with multiple proton resonances in the ligands corresponds to His-PIMA-ZW-QDs (i.e., bound ligands). Given the absence of signals on unbound ligands in the measured

spectrum, it indicates that following phase transfer and purification no measurable free ligands were left in the medium, further confirming the effectiveness of the ligand design and protocols used. The QD hydrodynamic radius (R_H) extracted from the diffusion coefficient using Stokes-Einstein equation, $D = k_B T/(6\pi\eta R_H)$, is ~5.2 nm; k_B is the Boltzmann constant, T is the absolute temperature (293 K) and η is the dynamic viscosity of the medium (~1 cP or 1.002×10^{-3} N s/m^2).[58,59] This value is in good agreement with the size extracted from dynamic light scattering ($R_H \cong 5.7$ nm), using the Laplace transform of the autocorrelation function (see Figure 2E). This size is comparable to that measured for DHLA-QDs. It is, however, smaller than the values measured for DHLA-PEG$_{750}$-QDs and for LA/His-PIMA-PEG-QDs with similar core radius: $R_H \cong 8$ nm for DHLA-PEG$_{750}$-QDs and $R_H \cong 11$ nm for LA/His-PIMA-PEG-QDs.[39,60] The rather compact size offered by this polymer-coating results from combining multi-coordination on the QDs and the use of the zwitterion motif, yielding homogeneous QDs with a very thin surface coating. Such thin coating is further confirmed by the ability to conjugate polyhistidine-tagged proteins onto these QDs (see below).

4) Estimation of the ligand density per QD. The above NMR data were exploited to extract an estimate for the density of polymer ligands on the nanocrystals, by comparing the total concentration of ligands to that of the QDs in the sample with added pyridine as a standard. The concentration of ligands was extracted by comparing the integrations of the methyl-proton in the polymer backbone to the α-proton in pyridine. The QD concentration was estimated from the absorbance at 350 nm.[7] Such analysis yielded a value of ~13.3 polymer ligands per QD emitting at 537 nm (radius ~3.0 nm, extracted from x-ray scattering).[61] This corresponds to ~260 imidazole anchoring groups per QD. We also used NMR data to estimate the number of amines and folic acid groups per QD when ligated with His-PIMA-ZW/NH_2 (10% amine) or His-PIMA-ZW/FA (10% folic acid). Overall, there are ~52 amines or folic acid groups per QD. Additional details about the ligand density estimates using ^{1}H NMR data are provided in the Supporting Information (see Figure S5).

Colloidal Stability Tests. The colloidal stability of aqueous QDs capped with His-PIMA-ZW was evaluated under several biologically relevant conditions, including a pH range 3-13, high ionic strength buffers (1 M NaCl), growth media (100% RPMI-1640), and storage of nanomolar dispersions (e.g., 10 nM) under room temperature and light exposure conditions.

Figure 3A shows the fluorescence images of green-emitting QDs dispersed in buffers at pH 5-13 and in 1 M NaCl buffer, stored at ~4 ˚C in the dark. All QD dispersions stayed stable for at least 12 months, with no sign of aggregation or loss of fluorescence. Additional data on the stability of QDs in pH 3 buffer are provided in the Supporting Information (Figure S6), where His-PIMA-ZW-QDs stayed stable for at least 5 weeks, though the fluorescence decreased after 3 weeks. This reduced stability at such low pH is expected, due to the protonation of imidazole (pKa of the imidazole ~6.0).[62] Similar observations have been reported for other imidazole-based ligands at pH $\leq$ 5.[23,48] For example, we have found that the dispersion of QDs coated with His-PIMA-PEG (PEGylated polymer) exhibit a progressive loss in the measured fluorescence at pH 3 after 1-month storage; nonetheless, photo-stability can be substantially improved by using mixed coordination ligands (LA/His-PIMA-PEG).[39] The colloidal stability of QDs was further assessed in the presence of endogenous thiols, namely glutathione and in cell growth media. Figure 3B shows the fluorescence images for QD dispersions in 10 mM glutathione solution and 100% growth media (RPMI-1640), with no aggregation build up or loss of fluorescence for 3 months of storage. The above results are very important for using such QDs to investigate intracellular media, rich in ions, proteins and reducing agents.

We complemented the above results by carrying out gel electrophoresis measurements of hydrophilic QDs to identify whether or not pH changes can affect the QD mobility and if the zwitterion coating provides net charges to the QD surface, in addition to those provided by the carboxy groups on the polymer backbone. Figure 3C shows that the fluorescent bands of the His-PIMA-ZW-QDs at pH 5-13 are narrow (with no observable smearing) and with an essentially identical mobility shift. In comparison, the bands measured for QDs coated with PEGylated polymer (i.e., LA/His-PIMA-PEG-QDs) are also narrow but have smaller mobility shift than those measured for His-PIMA-ZW-QDs (see Figure 3C). These results indicate that the dispersions are made of a uniform distribution of nanocrystal size and surface charge density across the pH range. They also imply that the zwitterion groups provide a net negative charge to the QDs, in addition to those provided by the carboxy groups. Furthermore, the density of surface charges for each coating is not affected by pH changes, as reflected by the identical mobility shift measured at each pH, albeit a larger shift measured for zwitterionic coating.[39] Previous reports have also shown that zwitterion moieties contribute a net negative charge attributed to the strong ionic signature of the sulfobetaine groups.[43,44]

We further tested the colloidal stability of His-PIMA-ZW-QDs at low concentrations and under room temperature and light exposure conditions. The fluorescence images in Figure 4A indicate that the QDs stayed stable for at least 4 months at all the concentrations used: 300 nM, 50 nM and 10 nM. The PL intensity measured for the 300 nM QD dispersion was essentially unchanged for at least 60 days. For the 50 nM and 10 nM dispersions the fluorescence emission was maintained for the first month, but gradually decreased after that. For example, losses of ~30% and ~50% were respectively measured for the 50 nM and 10 nM dispersions after 2 months (Figure 4B). In comparison, a pronounced reduction in the PL was measured for QDs photoligated with LA-PEG_{750}-OMe-QDs reported in reference.[44] The reduced stability of QDs capped with molecular thiol derivatives at small concentrations and over time has been attributed to possible thiol oxidation and ligand desorption from the QD surfaces.[23,38,39] Stability against oxidation was monitored for our newly-capped QDs when dispersed in a solution of hydrogen peroxide (H_2O_2). Figure 4C shows that the QD PL was essentially unaffected by the addition of H_2O_2 throughout the range of concentrations tested up to 240 μM, with the PL intensity remaining at 95%-100% of its initial value. In comparison, DHLA-PEG_{750}-OMe-QDs exhibited weaker resistance to H_2O_2, as indicated by a ~30% reduction in PL measured at 60-240 μM H_2O_2.

Overall the better colloidal stability at pH 5-13, to H_2O_2 oxidation, and in growth media proves a great tolerance of the His-PIMA-ZW-QDs to photo and chemical oxidation, a result that can be attributed to the enhanced coordination of the multi-imidazole ligands and the strong affinity of zwitterion moieties to water.

QD-Protein Conjugation. Direct immobilization of polyhistidine-appended biomolecules onto the nanocrystal surface, as a means of forming QD-bioconjugates driven by metal-affinity coordination, has been applied to attach peptides and proteins to core-shell QDs and AuNPs alike.[50,51,53,54,63] This is an attractive route due to the ease of implementation and the ubiquitous presence of His-tagged proteins expressed in bacteria, or synthetically-prepared peptides. However, one key requirement for such conjugation is to use small capping ligands so that the His-tag is able to directly reach to the nanocrystal surface. In our previous work, DHLA-capped QDs have been extensively used for conjugation with His-tagged proteins, but the colloidal stability of these nanocrystals was limited to basic conditions.[51-53] Here, we applied this conjugation strategy to the His-PIMA-ZW-capped QDs (emitting at 556 nm) using two proteins:

maltose binding protein appended with a N-terminus 7-histidine tag (MBP-His_7) and a fluorescent protein appended with a N-terminus 6-histidine tag (mCherry-His_6).

1) QD-MBP conjugates: amylose column assay. QD-MBP conjugation was tested using amylose chromatography, followed by competitive release with maltose (see Figure 5). Following incubation of MBP-His_7 with His-PIMA-ZW-QDs (ratio of MBP:QD = 12:1), the resulting QD-MBP conjugates were tightly bound onto the top of the amylose column (as indicated by the green fluorescent band observed under irradiation using a hand held UV lamp), and were not eluted even after three washes with buffer; this binding is promoted by the affinity of MBP to the amylose gel. Addition of 1 mL of 20 mM D-maltose, the substrate of MBP, readily resulted in elution of the conjugates. Binding to amylose and release by adding maltose, complemented with the fluorescence emission of the band, confirmed that the conjugation between MBP-His_7 and the polymer-capped QDs has taken place. We should note that conjugation of DHLA-QDs to His-tagged proteins has been accompanied by enhancement in the QD emission.[51,52] A similar trend was observed for our conjugates, with a progressive increase in the sample PL when the ratio of MBP-to-QD increased from 0:1 to 12:1 (see Supporting Information, Figure S7). However, this enhancement was much smaller compared with that measured for MBP-His_5 self-assembled onto DHLA-capped QDs.[51,52] For instance, only ~20% enhancement was measured for the His-PIMA-ZW-QDs conjugated with ~ 8 MBP-His_7, while an increase of ~90% was measured for the DHLA-QD with the same conjugate valence.[52] Such variance is probably due to the different nature of surface capping between the two sets of ligands. Thiol-appended ligand tends to lower QD PL, hence the effects of polyhistidine tag coordination are more pronounced.[40] In contrast, His-PIMA-ZW-QDs already have high PL signal with multi-imidazole coordination, limiting the enhancement effects of His-tagged protein conjugation.

2) QD-mCherry conjugates: FRET analysis. Self-assembly of the fluorescent mCherry protein appended with a His_6-tag onto His-PIMA-ZW-QDs was verified by evaluating the fluorescence resonance energy transfer (FRET) interactions. Figure 5B shows the absorption spectra of QD-mCherry-His_6 at a protein-to-QD ratio (conjugate valence) ranging from 0:1 to 12:1. The progressive increase in the absorption peak at ~586 nm is due to mCherry contribution. The corresponding composite emission spectra, collected using excitation at 400 nm, are shown in Figure 5C. Spectra show a progressive loss in QD emission accompanied with a gradual increase

in mCherry emission as the molar ratio of protein-to-QD increases. Since the fluorescence due to direct excitation of the mCherry is negligible (see purple profile in Figure 5C), we attribute the fluorescence contribution of mCherry in the composite spectra to FRET sensitization of the protein.

Values for the relative QD PL losses along with the FRET efficiencies, derived from the deconvoluted emission spectra as a function of conjugate valence, are shown in Figure 5D. The trends for both experimental parameters agree well with the predictions from the FRET interactions between one central donor surrounded by *n* equally-spaced acceptors. Using the expression of FRET efficiency for the above conjugate configuration, $E = nR_0^6/(nR_0^6 + r^6)$ (R_0 and r being the Förster radius and QD-to-mCherry center-to-center separation distance, respectively), we extract an experimental estimate for r of ~60 Å. This value is comparable to the value measured for mCherry-His_6 self-assembled onto QDs photoligated with bis(LA)-ZW ligands, but slightly larger than the value reported for mCherry self-assembled onto green-emitting DHLA-QDs (r ~56 Å).[44,64] Additional details on the FRET analysis along with the corresponding parameters are provided in the Supporting Information (Figure S8 and Table S1). We should note that in order to account for the small enhancement in QD PL upon conjugation to polyhistidine tagged proteins, the PL from dispersions of QD-MBP-His_7 conjugates were used as control/reference samples to calculate the experimental FRET efficiencies. This result is greatly promising to form self-assembled QD-protein conjugates, where control over valence and potentially protein orientation is easily achieved using this approach.

QD-Dopamine Conjugates as PL Sensing Platforms. It has been reported that oxidized dopamine can interact with the cysteine residues of parkin, a ligase protein that mediates the degradation of proteins toxic to dopaminergic neurons.[65] This covalent modification results in degeneration of nigral neurons over time, due to the inactivation of its ubiquitin ligase function. Meanwhile, the oxidative metabolism of dopamine has received a great attention in Parkinson's disease because it yields quinones, hydrogen peroxide and other reactive oxygen species (ROS), which could damage lipids, proteins, DNA and consequently lead to cell death.[66] Those studies also indicate that oxidative metabolism of dopamine is closely related with iron-catalysis and depletion of biothiol molecules (e.g., cysteine) to form 5-*S*-cysteinyl-dopamine.[67-69]

We tested some of these interactions by probing their effects on the fluorescence emission of QD-dopamine conjugates. For this we first reacted dopamine-isothiocyanate

(dopamine-ITC) with His-PIMA-ZW/NH_2-capped QDs to promote covalent attachment via isothiourea bond.[70] This produces sensing platforms where the fluorescence emission can be modulated by charge transfer (CT) interactions between the QD and proximal dopamines.[70] We used these conjugates to probe: changes in the buffer pH, effects of added iron ions, and interactions with cysteine amino acid. Figure 6 shows a schematic representation of the proposed modulation of the QD PL via four distinct pathways: 1) pH-induced PL changes which are attributed to a change in the oxidization potential of catechol with increasing pH, combined with a shift in the chemical equilibrium between dopamine catechol (reduced form) and dopamine quinone (oxidized form).[70] 2) Interactions of QD-dopamine dispersed in pH 10 buffer with cysteine. Here, the thiol group of cysteine reacts with quinone (dominant at pH 10) to form 5-*S*-cysteinyl-dopamine. This reaction produces a QD PL recovery, due to a reduction in the charge transfer interactions with the QDs, as the concentration of quinone in the medium is decreased. 3) Interactions of QD-dopamine with Fe ions in DI water, where Fe-catalyzed oxidation of dopamine increases the concentration of quinone, thus enhancing electron transfer interactions from QDs. This results in pronounced PL loss that directly traces the concentration of added Fe ions. 4) Effects of competing interactions between cysteine and QD-dopamine premixed with Fe ions. The added of cysteine molecules compete with Fe ions for interactions with quinone, promoting a reverse transformation to 5-*S*-cysteinyl-dopamine. This transformation alters the nature of QD-to-dopamine interactions, resulting in QD PL recovery.

1) pH-dependent quenching of QD fluorescence. Figure 7A shows the PL spectra collected for the set of QD-dopamine conjugates when the buffer pH was changed from 4 to 10; a progressive quenching was observed when pH was shifted from acidic to basic. These intermediate valence conjugates were prepared using 50 μL of dopamine-ITC during the coupling reaction, see experimental section. Cumulative plots for the progression of the normalized PL with pH for all three sets of conjugates prepared with different dopamine-to-QD molar ratio are shown. Similar quenching behavior was measured for all three dispersions, albeit the quenching was more pronounced for samples prepared with higher conjugate valence. In comparison, no change in the QD PL was measured for the control sample made of QDs alone. These results are consistent with previous data prepared with QDs capped with DHLA-PEG ligands.[70-72] The progressive PL loss with increasing pH can be attributed to CT interactions between the QD and dopamine. Such

interactions involve complex electron and hole exchange between photoexcited QDs and a mixture of reduced (catechol) and oxidized (quinone) forms of dopamine.[71,72]

2) Probing the interactions between QD-dopamine conjugates and cysteine. We utilized the above QD-dopamine conjugates to probe interactions with cysteine; cysteine solution was added to a dispersion of QD-dopamine preset at pH 10. Figure 7B shows the QD PL changes with the reaction time when QD-dopamine conjugates were dispersed in the presence of 8 μM cysteine. The QD PL exhibited a progressive increase with time until saturation. Moreover, the normalized PL intensities at saturation were concentration-dependent. These results indicate that transformation from quinone to 5-*S*-cysteinyl-dopamine was faster in the presence of higher concentrations of cysteine (faster reaction kinetics). Control experiments (QDs alone, no conjugated dopamine) showed marginal change in PL signal. This indicates that our polymer-coated QDs are neither pH-sensitive nor affected by potential cysteine competition for surface coordination (see Supporting Information Figure S9).

3) Sensing Fe ions with QD-dopamine conjugates. Figure 7C shows the PL spectra together with a plot of the normalized PL data collected from dispersions of QD-dopamine conjugates mixed with varying concentrations of Fe ions ranging from 0 μM to 20 μM. The QD-dopamine conjugates were prepared by reacting the polymer-QDs with 25 μL of dopamine-ITC. A linear decrease in the PL is measured when the iron concentration is increased in the tested range, see Figure 7C.

4) Competitive binding of cysteine to quinone. Addition of cysteine to the above dispersions containing QD-dopamine conjugates pre-mixed with Fe ions was found to induce a partial recovery of the QD PL as shown in Figure **7**D. This is attributed to competition between the cysteine and Fe ions for interaction with the conjugates, which induces a reverse transformation from quinone (produced by Fe-catalysis) to 5-*S*-cysteinyl-dopamine. Nonetheless, recovery is not full as a fraction of the Fe and cysteine may still interact simultaneously with dopamine, forming 5-cysteinyl-dopamine-Fe complex; this configuration would still produce partial quenching of QD PL. Additional details about the CT charge transfer interactions involved are provided in the Supporting Information (Figure S11).

Intracellular Delivery of Folic Acid-Decorated QDs. The folate receptor protein is a biomarker commonly overexpressed on the membrane of breast, lung, kidney and ovary

epithelial cancer cells.[73,74] It has high affinity for folic acid (with a reported dissociation constant, $K_D \cong 0.1$ nM) and it promotes its intracellular transport via receptor-mediated endocytosis.[73,75,76] This uptake mechanism has been exploited to promote the intracellular uptake of folic acid-conjugated nanoparticles and drugs, as well as for use in tumor-targeting, imaging and anticancer therapy.[73,77,78] Here, we demonstrate that our folic acid-modified ligand (His-PIMA-ZW/FA) can promote the delivery of large amounts of QDs into live cells.

Figure 8A shows the epifluorescence images collected for HeLa cells co-incubated with QD-His-PIMA-ZW/FA (QD-FA, 200 nM) and Texas Red-transferrin (0.5 μM) for 1 hour. The images in panel A correspond to the QD emission (green), Texas Red-transferrin endolysosomal marker (red), a merged composite fluorescence image with the DAPI staining of the nuclei (blue), along with an image superposing fluorescence and differential interference contrast (DIC). Images show the presence of punctate QD fluorescence distributed in the perinuclear region, with no apparent nuclear staining. The QD fluorescence was mostly co-localized with the distribution of endo/lysosomal compartments shown in the merged images, indicating that the QD-FA conjugates have been mainly internalized via folate-mediated endocytosis. In comparison, control experiments carried out using cells incubated with QD-His-PIMA-ZW (no folic acid) showed no intracellular QD fluorescence (see Supporting Information, Figure S12).

To probe the efficiency of folic acid-mediated internalization, we incubated cells with QD-FA conjugates at different concentrations and for different time intervals. Figure 8B shows three representative fluorescence images collected for HeLa cells incubated with 100, 150, and 200 nM QD-FA conjugates for 1 hour. Images clearly show that the intracellular uptake of QDs was concentration-dependent, with the highest fluorescence observed for cells incubated with 200 nM conjugate dispersions. Similarly, higher intracellular staining was measured for cells incubated with QD-FA conjugates for longer time (see Figure 8C), indicating that uptake is also time-dependent. These results combined prove that folic acid-modified polymer ligand promote specific cellular internalization of QDs in concentration- and time-dependent manner.

Cellular Uptake of QD-Transferrin Conjugates. Here, we tested the intracellular uptake of QDs conjugated to the protein receptor transferrin after phase transfer to buffer. For this, we started with QDs capped with His-PIMA-ZW ligands. The carboxylic acid groups along the PIMA backbone were then activated with EDC/NHS, followed by reaction with lysine amino acids of transferrin (via carboxyl-to-amine crosslinking),[79] as illustrated in Figure 9A. The QD-

transferrin conjugates were separated from byproducts using PD-10 size exclusion column, then incubated with HeLa cells at 200 nM for 1 hour. These cells were washed twice with PBS buffer and subsequently incubated with 0.5 μM TR-Tf (as endosome marker) for an additional 40 min. Figure 9B shows that the QD-green signal was observed for the cells incubated with the QD-transferrin, and that the distribution is fully co-localized with that of TR-Tf marker, indicating that here too the uptake is via endocytosis. Control experiments indicate that incubation of cells with unconjugated QDs at the same concentration resulted in no intracellular signal (data not shown).

These findings combined indicate that the prepared polymer-coated QDs can be reacted post phase transfer with specific proteins or peptides via either metal-polyhistidine conjugation or covalent coupling to yield bio-reactive conjugates. Alternatively, biomolecules can be introduced in the polymer structure in-situ during the ligand synthesis prior to ligand exchange on the nanocrystal. The conjugates prepared via either route can be effectively used in applications such as sensing, cellular uptake and imaging.

We would like to provide a contextual comparison between the PEG-based polymer ligands reported in reference 39 (namely, LA/His-PIMA-PEG) and the one prepared and tested in this report (i.e., His-PIMA-ZW). Even though the chemical design to prepare the ligands is similar, relying on the efficient nucleophilic addition reaction starting form poly(isobutylene-*alt*-maleic anhydride), there are a few key differences that influence the QD behavior in buffer media. The present ligand design takes advantage of the effective anhydride reactivity towards amine-presenting molecules, but substitutes zwitterion moieties for short PEG chains and uses only imidazole anchors for coordination onto the QD surface. This has yielded QDs with high PL yields in buffer media (comparable to those measured for hydrophobic QDs), and more importantly very compact overall dimensions. The R_H value measured here is comparable to that measured for DHLA-QDs, which is remarkable for a polymer coating strategy. The coating yields a net negative charge density, resulting from contribution of the carboxy groups freed during the reaction and the newly introduced sulfobetaine groups; these groups tend to stay negatively charged even in acidic buffers. The similar mobility for the QD dispersions over the pH range (5-13) shown in Figure 3C indicates that there are no pH effects on the overall charge distribution of His-PIMA-ZW-QDs. Finally, the use of only imidazole coordination combined with ZW solubilizing moieties provides nanocrystals that are fully compatible with the metal-

histidine self-assembly of polyhistidine-tagged full size proteins on the QDs. This is very promising for potential use in biology. Nonetheless, the absence of lipoic acid anchors from the His-PIMA-ZW ligands provided less optimal colloidal stability in acidic conditions, consistent with the PEGylated polymer with imidazole anchors only (i.e., His-PIMA-PEG).

Conclusion

We have developed a new set of metal-coordinating polymer ligands combining the imidazole anchoring group with the hydrophilic zwitterion motif and used them for the surface-functionalization of luminescent QDs. The ligand design exploits the highly efficient nucleophilic addition reaction between poly(isobutylene-*alt*-maleic anhydride), PIMA, and amines, and was used to introduce a controllable number of imidazole anchors, hydrophilic zwitterion moieties, along with reactive groups on the same polymer chain. We have further exploited this addition reaction to introduce biomolecules (such as folic acid as cancer cell targeting agent) into the polymer ligands prior to ligation on the QDs. This expands on our previous work using the PIMA precursor to prepare other PEG-based ligands; those ligands were used to functionalize iron oxide nanoparticles, QDs and AuNPs.[39,55,80]

Ligation with these polymers has yielded hydrophilic QDs that exhibit excellent colloidal stability over a broad range of biological conditions, including storage at very low concentrations and under ambient conditions and a resistance against chemical oxidation by H_2O_2. This very thin hydrophilic coating afforded by zwitterion motif yields QDs with small hydrodynamic radius (R_H ~ 5-6 nm), allowing conjugation with polyhistidine-tagged proteins via metal-affinity coordination. We have also shown that coupling of dopamine onto the QDs provides fluorescent platforms that can sense changes in pH of the medium, the presence of Fe ions, and interactions with cysteine. Finally, we found that QDs ligated with folic acid-modified polymer could promote the effective delivery of large amounts of QDs into living cancer cells via folate receptor-mediated endocytosis.

These results are greatly promising for fluorescent labeling in biology, including cellular imaging and sensing, where probes that are small in size and stable at very low concentrations are often required. Conjugates prepared with such nanocrystals would find great use to image blood vasculature and for tracking protein migration in live cells and tissues. We also anticipate that this chemical design would be applicable to prepare additional polymers with other functionalities adapted to different inorganic nanocrystals. This nucleophilic addition reaction can be easily used to develop various functional polymers with potential applications in antifouling coating and for chelation to transition metal surfaces.

Experimental Section

Synthesis of His-PIMA-ZW. In a 50-mL three-neck round-bottom flask equipped with an addition funnel and a magnetic stirring bar, 0.385 g of poly(isobutylene-*alt*-maleic anhydride) (PIMA, MW ~ 6000 g/mol, 2.5 mmol of monomer units) was dissolved in 5 mL of DMSO. The solution was purged with nitrogen for 10 min and then heated to 45 ˚C. Histamine (0.139 g, 1.25 mmol) was dissolved in 1 mL of DMSO using a scintillation vial, and this content was added dropwise to the PIMA solution through the addition funnel. After that, 1 mL of DMSO solution containing ZW-NH_2 (0.280 g, 1.25 mmol) was added, and the reaction mixture was left stirring at 45 ˚C overnight. The solution was concentrated to ~2 mL under vacuum, and large excess of acetone was added to precipitate the compound, followed by centrifugation. The solid pellet was washed 3 times with acetone and then dried under vacuum, producing the final product as white powder; the reaction yield was ~ 93%.

Synthesis of His-PIMA-ZW/NH_2 (10% amine). PIMA (0.385 g, 2.5 mmol of monomers) was dissolved in 5 mL of dry DMSO using a 50-mL round-bottom flask equipped with an addition funnel and a magnetic stirring bar. The solution was purged with nitrogen for 10 min and then heated to 45 ˚C. To the stirring solution, 1 mL of DMSO containing histamine (0.139 g, 1.25 mmol) was added dropwise through the addition funnel, followed by 1 mL of DMSO containing ZW-NH_2 (0.224 g, 1 mmol). After 2 hours, H_2N-PEG-NH_2 (0.15 g, 0.25 mmol) dissolved in 1 mL of DMSO were finally added to the reaction mixture. Once the addition was complete, the mixture was stirred at 45 ˚C overnight. The solvent was then removed under vacuum and the compound was precipitated by adding large excess of acetone. After centrifugation, the solid pellet was washed with acetone and dried under vacuum. The final compound was a yellowish solid, with a reaction yield of ~ 85%.

Synthesis of His-PIMA-ZW/FA (10% folic acid). In 50-mL three-neck round-bottom flask equipped with a magnetic stirring bar, PIMA (0.15 g, 0.975 mmol of monomers) was dissolved in 3 mL of DMSO, then the solution was purged with nitrogen for 10 min while stirring. To this solution, 1 mL of DMSO containing histamine (0.0542 g, 0.487 mmol) was added dropwise using a syringe. This was followed by the stepwise addition of 1 mL of folic acid solution in DMSO (0.043 g, 0.097 mmol), and 1 mL of DMSO containing ZW-NH_2 (0.087 g, 0.39 mmol). The reaction mixture was further stirred at room temperature overnight, and then concentrated to

~ 1 mL under vacuum. The compound was precipitated by adding excess acetone and centrifuged for 3 min at 3700 RPM. The resulting solid pellet was washed with acetone and dried under vacuum, yielding a yellow powder; the reaction yield was ~ 86%.

Synthesis of the QDs. The nanocrystals used in this study were made of CdSe-ZnS core-shell, grown via reduction of organometallic precursors at high temperature in a hot coordinating solvent mixture, in two steps: growth of the CdSe core followed by ZnS-overcoating. Growth of the CdSe core involved the reduction of cadmium and selenium precursors at high temperature in a hot (300-350 °C) coordinating solvent mixture made of trioctyl phosphine (TOP), trioctyl phosphine oxide (TOPO), alkylamines and alkylcarboxyls; the nanocrystal core size was controlled by adjusting the precursor concentrations and temperature. Overcoating the CdSe core with ZnS shell using zinc was carried out at lower temperature. The QD sizes were tuned by varying the CdSe core radius, while maintaining the same overcoating ZnS layer. A detailed description of the QD growth (both core and shell) is provided in the Supporting Information.

Ligand Exchange. We limit our description to the preparation of QDs capped with His-PIMA-ZW. The same protocol is applicable to capping with the other ligands. A solution of hydrophobic QDs (26.7 μM, 150 μL) was precipitated using ethanol and redispersed in 200 μL of chloroform. Separately, 15 mg of His-PIMA-ZW was dissolved in 200 μL of DMSO with gentle heating and sonication (for ~3-5 min). The ligand solution and the QD dispersion were then mixed in scintillation vial. The vial was sealed with a rubber septum and the atmosphere was switched to nitrogen by applying 2 to 3 rounds of mild vacuum; the mixture was then left stirring at room temperature overnight. The QDs were precipitated by adding 500 μL of hexane and acetone (in excess). Following sonication for ~1 min, the solution was centrifuged at 3700 RPM for ~5 min, yielding a pellet. The procedure was repeated one more time. The final precipitate was dried under vacuum for ~10 min to yield a powder, which could then be readily dispersed in 3-5 mL of phosphate buffer (pH 12, 50 mM); sonication for ~5 min may be needed to fully disperse the powder. The obtained clear aqueous dispersion of QDs was filtered through a 0.45 μM syringe filter, and excess free ligands were removed by applying 3-4 rounds of concentration/dilution with DI water using a centrifugal filtration device (Millipore, MW cutoff = 50 kDa). This protocol has provided clear QD dispersions, e.g., ~500 μL with a concentration of ~7-8 μM. Ligand exchange with His-PIMA-ZW/NH_2 or with His-PIMA-ZW/FA was carried

out following the same steps, except that the amount of polymer ligands used was ~ 20 mg for both cases.

Remark: *When the ligand solution was mixed with the QD dispersion in an organic mixture, the solution progressively became turbid due to the limited solubility of zwitterion moieties in the polymer coating.*

NMR Sample Preparation. We used pulsed-field gradient water suppression to collect the ^{1}H NMR spectra. Briefly, after ligand exchange and phase transfer of the QDs (as described above), the DI water was switched to D_2O by applying two rounds of concentration/dilution using deuterium oxide (2 mL each). The final volume of the QD dispersions in D_2O used to collect the NMR spectra was adjusted to 500 μL and the concentration was ~8-9 μM. The ^{1}H NMR spectra were collected by averaging over 500 scans. The same sample was used for collecting the ^{31}P NMR spectrum of His-PIMA-ZW-QDs in D_2O. The ^{31}P NMR spectrum of the native hydrophobic QDs was collected from the dispersion prepared from growth solution by purification via one-round precipitation with excess ethanol, drying under vacuum, and re-dispersion in chloroform-d ($CDCl_3$). The concentration was ~10 μM.

The samples used for surface ligand counting experiments were prepared following the same protocol, but 2 μL of pyridine (24.8 μmol) dissolved in 5 μL of D_2O was added to the QD dispersion as standard. We should note that the final QD concentration in the NMR sample was slightly altered with the addition of pyridine (e.g., addition of pyridine reduced the QD concentration from ~8.6 μM to ~8.5 μM).

Assembly of QD-Protein Conjugates. Two different proteins were used for conjugation onto the QDs via metal-histidine promoted self-assembly: maltose binding protein appended with a 7-histidine sequence (MBP-His_7) and the fluorescent mCherry protein appended with a 6-histidine sequence (mCherry-His_6); both sequences were inserted at the N-terminus.[63] The protein expression and purification, briefly summarized in the Supporting Information, were carried out following the protocols detailed in reference.[63] The conjugation was carried out using the same steps for both proteins. Here we detail the assembly of QD-mCherry conjugates with varying valence. ~22.2 μL aliquots of a stock QD dispersion (3.6 μM) were loaded into Eppendorf tubes and the volume in each tube was adjusted by adding phosphate buffer (pH 8.0, 40 mM) to 100

μL. The desired amounts of mCherry solutions were loaded into separate tubes, followed by the addition of phosphate buffer to bring the total volume to 300 μL. The ratio of mCherry-to-QD (i.e., valence) explored in this study was varied from 0.5:1 to 12:1. For example, dispersion with a valence of ~1 was prepared by adding ~6.2 μL of mCherry stock solution (12.9 μM) to 294 μL of phosphate buffer, followed by gentle mixing with the QD dispersion and incubation at 4 ˚C for 30 min to allow for self-assembly. The samples were then characterized by collecting the absorption and emission spectra.

QD-Dopamine Conjugates. Freshly prepared QDs capped with His-PIMA-ZW/NH_2 (10% amine) were reacted with dopamine-ITC to provide the final QD-dopamine conjugates.[70] We prepared three sets of conjugate dispersions by reacting the His-PIMA-ZW/NH_2-QDs with different amounts of dopamine-ITC. The first set was prepared by adding 25 μL aliquots of dopamine-ITC pre-dissolved in DMSO (0.5 mg/mL) to scintillation vials containing 136 μL of QD dispersion (~5.90 μM) and 20 μL NaCl solution (1 M); DI water was then added to bring the total volume to ~1 mL. The mixtures were then stirred for ~3 h in the dark, followed by removal of excess free/unreacted dopamine using one round of concentration/dilution through a membrane filtration device (MW cutoff: 50 kDa, Millipore) to provide the final conjugate dispersions (1 mL and ~0.8 μM QD concentration). For the other two samples, 50 μL and 100 μL aliquots of dopamine-ITC were reacted with the QD dispersions.

1) pH-dependent quenching of QD fluorescence. The pH-dependent PL quenching data were collected for all three sets of conjugates with QD-dopamine concentration of ~32 nM. These were prepared by mixing aliquots (40 μL) of the conjugate stock dispersions with 960 μL of phosphate buffer (10 mM) at the desired pH. The florescence spectra were collected for each sample, and the integrated PL signal was reported relative to the value measured at pH 4.

2) Interactions of QD-dopamine with soluble cysteine. The stock dispersions of QD-dopamine conjugates used in these experiments were prepared using 50 μL of dopamine-ITC (intermediate dopamine valence). 40 μL aliquots of the QD-dopamine conjugates were first dispersed in phosphate buffer (pH 10, 10 mM), then the desired volumes of cysteine stock solution (concentration = 0.1 mM) were added. The final volume of solutions was adjusted to 1 mL by adding the required amounts of pH 10 buffer. The cysteine concentrations used in these

measurements were 1, 4, and 8 μM (i.e., excess cysteine). The mixtures were incubated for different time periods and the PL spectra were recorded after each period.

3) Fluorescence sensing of Fe ions using QD-dopamine conjugates. Here, we started with the dispersions of QD-dopamine conjugates having the lowest valence (dispersions of conjugates prepared using 25 μL of dopamine-ITC). The conditions used for conjugation of QDs to dopamine-ITC were identical to those described above, except that the DI water was purged with argon for ~20 min.[70] Separately, a stock solution of Fe ion (2 mM) was freshly prepared by dissolving $FeCl_3 \bullet 6H_2O$ in DI water. Then, aliquots of the QD-dopamine dispersions (50 μL) were diluted in DI water and mixed with the desired volume of Fe solution. The final total volume of the mixture was 1.5 mL. The concentration of QD-dopamine was fixed at ~26.7 nM, while that of Fe ions was varied from 0 to 20 μM. The PL spectrum was collected for each dispersion and the intensity was plotted versus the Fe ion concentration and reaction time.

4). Cysteine-induced PL recovery of QD-dopamine-Fe-complex conjugates. We start with a dispersion of QD-dopamine pre-mixed with Fe ions, i.e., quenched QD PL. This dispersion was prepared by diluting 50 μL of QD-dopamine conjugates in 1.423 mL of DI water, followed by the addition of 15 μL of Fe solution (2 mM). Then, 12 μL of cysteine was added to above solution and mixed. The final total volume of the dispersion was 1.5 mL, while the final concentrations of Fe and cysteine were 20 μM and 8 μM, respectively. The PL spectra were recorded from the sample at different time intervals. We started with Fe concentration that gave us the highest quenching (see above).

Preparation of QD-transferrin Conjugates. To prepare the QD-transferrin conjugates, the carboxylic groups available on the His-PIMA-ZW-QDs (freed during the addition reaction) were reacted with the amine groups of transferrin, via EDC/NHS condensation reaction.[79] Briefly, 50 μL of His-PIMA-ZW-capped QDs (7.22 μM) were first dispersed in 400 μL of phosphate buffer (pH = 6.5, 50 mM), and then 100-fold excess of NHS (8.5 mM, 4.2 μL) and EDC (5 mM, 7.2 μL) dissolved in DI water was added. The reaction was left to proceed for ~3 hours at room temperature, then the excess EDC and NHS were removed by applying one round of concentration/dilution with DI water using a membrane filtration device (MW cutoff: 50 kDa, Millipore). The purified QD-NHS esters were added to 400 μL of phosphate buffer (pH = 7.8, 20 mM) containing ~20-fold excess of transferrin (0.58 mg, MW = 80 kDa) with respect to the QD

concentration, and the mixture was incubated at 4 °C overnight. The conjugates were separated from unbound transferrin and NHS byproducts via size exclusion chromatography using PD 10 column. The first eluted fraction containing the QD-transferrin conjugates was used for the cellular uptake experiments.

Cell Imaging. HeLa cell cultures (human cervix carcinoma cell line), provided by the FSU cell culture facility, were grown at 37 ˚C in a humidified 5% CO_2 atmosphere at 37 ˚C, as a monolayer in a complete growth medium (Dulbecco's Modified Eagle's Medium, DMEM, Cellgro), supplemented with 10% (v/v) fetal bovine serum (Gibco), 4.5 g/L glucose, L-glutamine, sodium pyruvate, 1% (v/v) antibiotic-antimycotic 100x (Gibco), and 1% (v/v) non-essential amino-acid solution 100x (Sigma). 8 x 10^4 of the above cells were seeded onto 12 mm round micro-cover glasses in a 24-well microplate (CellStar, VWR). The plates were placed in an incubator for 24 hours to allow for cell attachment. The cells were then incubated with QD-FA or QD-transferrin conjugates and Texas Red labeled transferrin (at a concentration of ~0.5 μM). The QD concentrations and incubation times were adjusted according to the experimental needs. After incubation the cells were washed with PBS buffer twice, fixed with 3.7% paraformaldehyde and stained with 4,6-diamino-2-phenylindole (Prolong Antifade mounting media with DAPI nuclear staining, Invitrogen). Control experiments were carried out by incubating the cells with polymer-coated QDs (without folic acid or transferrin). The fluorescence images were acquired using an Inverted Nikon Eclipse Ti Microscope equipped with a color CoolSNAP HQ2 CCD camera. Excitation of the sample was provided by a Xe lamp, while the fluorescence images were collected using a 60x objective (Nikon) and a set of filter cubes from Chroma Technology (Rockingham, VT). The DAPI fluorescence was detected using a DAPI cube (with 340-380 nm excitation and 435-485 nm emission), the QD signal was detected using a GFP/EGFP cube (with 450-490 nm excitation and 500-550 nm emission), and the Texas Red-transferrin florescence was detected using a TEXAS RED HYQ cube (with 532-587 nm excitation and 608-683 nm emission).

Acknowledgements: The authors thank FSU and the National Science Foundation for financial support (NSF-CHE #1508501 and #1058957).

Supporting Information Available: Materials, instrumentations, additional experimental details, synthesis of amino-zwitterion, ^{1}H NMR characterization of ZW-NH_2, optical characterization of additional His-PIMA-ZW-capped QDs, ^{31}P spectra of QDs capped with TOP/TOPO/HPA and His-PIMA-ZW, additional ^{1}H NMR spectra of His-PIMA-ZW/FA-QDs and His-PIMA-ZW-QDs, FRET analysis, control experiments for sensing cysteine and iron ions, and control experiment of cellular uptake of QDs alone. This material is available free of charge via the Internet at http://pubs.acs.org.

References

(1) Murray, C. B.; Norris, D. J.; Bawendi, M. G. *J Am Chem Soc* **1993**, *115*, 8706.

(2) Alivisatos, A. P. *The Journal of Physical Chemistry* **1996**, *100*, 13226.

(3) C.B. Murray, C. R. K., M.G. Bawendi *Ann. Rev. Mater. Sci.* **2000**, *30*, 545.

(4) Peng, Z. A.; Peng, X. G. *J Am Chem Soc* **2001**, *123*, 183.

(5) Talapin, D. V.; Rogach, A. L.; Kornowski, A.; Haase, M.; Weller, H. *Nano Lett* **2001**, *1*, 207.

(6) Hines, M. A.; Guyot-Sionnest, P. *Journal of Physical Chemistry* **1996**, *100*, 468.

(7) Dabbousi, B. O.; RodriguezViejo, J.; Mikulec, F. V.; Heine, J. R.; Mattoussi, H.; Ober, R.; Jensen, K. F.; Bawendi, M. G. *J Phys Chem B* **1997**, *101*, 9463.

(8) Reiss, P.; Bleuse, J.; Pron, A. *Nano Lett* **2002**, *2*, 781.

(9) Wu, X. Y.; Liu, H. J.; Liu, J. Q.; Haley, K. N.; Treadway, J. A.; Larson, J. P.; Ge, N. F.; Peale, F.; Bruchez, M. P. *Nature Biotechnology* **2003**, *21*, 41.

(10) Michalet, X.; Pinaud, F.; Bentolila, L.; Tsay, J.; Doose, S.; Li, J.; Sundaresan, G.; Wu, A.; Gambhir, S.; Weiss, S. *Science* **2005**, *307*, 538

(11) Zrazhevskiy, P.; Sena, M.; Gao, X. H. *Chemical Society Reviews* **2010**, *39*, 4326.

(12) Chou, L. Y. T.; Ming, K.; Chan, W. C. W. *Chemical Society Reviews* **2011**, *40*, 233.

(13) Freeman, R.; Willner, I. *Chemical Society Reviews* **2012**, *41*, 4067.

(14) Kairdolf, B. A.; Smith, A. M.; Stokes, T. H.; Wang, M. D.; Young, A. N.; Nie, S. M. *Annu Rev Anal Chem* **2013**, *6*, 143.

(15) Kim, C. S.; Duncan, B.; Creran, B.; Rotello, V. M. *Nano Today* **2013**, *8*, 439.

(16) Sapsford, K. E.; Algar, W. R.; Berti, L.; Gemmill, K. B.; Casey, B. J.; Oh, E.; Stewart, M. H.; Medintz, I. L. *Chemical Reviews* **2013**, *113*, 1904.

(17) Howes, P. D.; Chandrawati, R.; Stevens, M. M. *Science* **2014**, *346*.

(18) Lemon, C. M.; Curtin, P. N.; Somers, R. C.; Greytak, A. B.; Lanning, R. M.; Jain, R. K.; Bawendi, M. G.; Nocera, D. G. *Inorg Chem* **2014**, *53*, 1900.

(19) Palui, G.; Aldeek, F.; Wang, W. T.; Mattoussi, H. *Chemical Society Reviews* **2015**, *44*, 193.

(20) Silvi, S.; Credi, A. *Chemical Society Reviews* **2015**, *44*, 4275.

(21) Choi, H. S.; Liu, W.; Misra, P.; Tanaka, E.; Zimmer, J. P.; Ipe, B. I.; Bawendi, M. G.; Frangioni, J. V. *Nature Biotechnology* **2007**, *25*, 1165.

(22) Baker, M. *Nat Meth* **2010**, *7*, 957.

(23) Liu, W. H.; Greytak, A. B.; Lee, J.; Wong, C. R.; Park, J.; Marshall, L. F.; Jiang, W.; Curtin, P. N.; Ting, A. Y.; Nocera, D. G.; Fukumura, D.; Jain, R. K.; Bawendi, M. G. *J Am Chem Soc* **2010**, *132*, 472.

(24) Giovanelli, E.; Muro, E.; Sitbon, G.; Hanafi, M.; Pons, T.; Dubertret, B.; Lequeux, N. *Langmuir* **2012**, *28*, 15177.

(25) Han, H. S.; Martin, J. D.; Lee, J.; Harris, D. K.; Fukumura, D.; Jain, R. K.; Bawendi, M. *Angewandte Chemie* **2013**, *52*, 1414.

(26) Cai, E.; Ge, P.; Lee, S. H.; Jeyifous, O.; Wang, Y.; Liu, Y.; Wilson, K. M.; Lim, S. J.; Baird, M. A.; Stone, J. E.; Lee, K. Y.; Davidson, M. W.; Chung, H. J.; Schulten, K.; Smith, A. M.; Green, W. N.; Selvin, P. R. *Angewandte Chemie International Edition* **2014**, *53*, 12484.

(27) Mattoussi, H.; Palui, G.; Na, H. B. *Adv Drug Deliver Rev* **2012**, *64*, 138.

(28) Dahan, M.; Levi, S.; Luccardini, C.; Rostaing, P.; Riveau, B.; Triller, A. *Science* **2003**, *302*, 442.

(29) Dubertret, B.; Skourides, P.; Norris, D. J.; Noireaux, V.; Brivanlou, A. H.; Libchaber, A. *Science* **2002**, *298*, 1759.

(30) Susumu, K.; Uyeda, H. T.; Medintz, I. L.; Pons, T.; Delehanty, J. B.; Mattoussi, H. *J Am Chem Soc* **2007**, *129*, 13987.

(31) Yu, W. W.; Chang, E.; Falkner, J. C.; Zhang, J. Y.; Al-Somali, A. M.; Sayes, C. M.; Johns, J.; Drezek, R.; Colvin, V. L. *J Am Chem Soc* **2007**, *129*, 2871.

(32) Liu, W.; Howarth, M.; Greytak, A. B.; Zheng, Y.; Nocera, D. G.; Ting, A. Y.; Bawendi, M. G. *J Am Chem Soc* **2008**, *130*, 1274.

(33) Yildiz, I.; McCaughan, B.; Cruickshank, S. F.; Callan, J. F.; Raymo, F. M. *Langmuir* **2009**, *25*, 7090.

(34) Lees, E. E.; Nguyen, T. L.; Clayton, A. H. A.; Mulvaney, P.; Muir, B. W. *ACS Nano* **2009**, *3*, 1121.

(35) Lin, C. A. J.; Sperling, R. A.; Li, J. K.; Yang, T. Y.; Li, P. Y.; Zanella, M.; Chang, W. H.; Parak, W. G. J. *Small* **2008**, *4*, 334.

(36) Thiry, M.; Boldt, K.; Nikolic, M. S.; Schulz, F.; Ijeh, M.; Panicker, A.; Vossmeyer, T.; Weller, H. *ACS Nano* **2011**, *5*, 4965.

(37) Zhang, F.; Lees, E.; Amin, F.; Gil, P. R.; Yang, F.; Mulvaney, P.; Parak, W. J. *Small* **2011**, *7*, 3113.

(38) Nagaraja, A. T.; Sooresh, A.; Meissner, K. E.; McShane, M. J. *ACS Nano* **2013**, *7*, 6194.

(39) Wang, W.; Kapur, A.; Ji, X.; Safi, M.; Palui, G.; Palomo, V.; Dawson, P. E.; Mattoussi, H. *J Am Chem Soc* **2015**, *137*, 5438.

(40) Bullen, C.; Mulvaney, P. *Langmuir* **2006**, *22*, 3007.

(41) Mattoussi, H.; Cheon, J. *Inorganic nanoprobes for biological sensing and imaging*; Artech House: Boston, 2009.

(42) Muro, E.; Pons, T.; Lequeux, N.; Fragola, A.; Sanson, N.; Lenkei, Z.; Dubertret, B. *J Am Chem Soc* **2010**, *132*, 4556.

(43) Park, J.; Nam, J.; Won, N.; Jin, H.; Jung, S.; Jung, S.; Cho, S. H.; Kim, S. *Advanced Functional Materials* **2011**, *21*, 1558.

(44) Zhan, N. Q.; Palui, G.; Safi, M.; Ji, X.; Mattoussi, H. *J Am Chem Soc* **2013**, *135*, 13786.

(45) Sun, M. H.; Yang, L. K.; Jose, P.; Wang, L.; Zweit, J. *J Mater Chem B* **2013**, *1*, 6137.

(46) Garcia, K. P.; Zarschler, K.; Barbaro, L.; Barreto, J. A.; O'Malley, W.; Spiccia, L.; Stephan, H.; Graham, B. *Small* **2014**, *10*, 2516.

(47) Susumu, K.; Oh, E.; Delehanty, J. B.; Blanco-Canosa, J. B.; Johnson, B. J.; Jain, V.; Hervey, W. J.; Algar, W. R.; Boeneman, K.; Dawson, P. E.; Medintz, I. L. *J Am Chem Soc* **2011**, *133*, 9480.

(48) Zhang, P.; Liu, S.; Gao, D.; Hu, D.; Gong, P.; Sheng, Z.; Deng, J.; Ma, Y.; Cai, L. *J Am Chem Soc* **2012**, *134*, 8388.

(49) Viswanath, A.; Shen, Y.; Green, A. N.; Tan, R.; Greytak, A. B.; Benicewicz, B. C. *Macromolecules* **2014**, *47*, 8137.

(50) Ghadiali, J. E.; Cohen, B. E.; Stevens, M. M. *ACS Nano* **2010**, *4*, 4915.

(51) Mattoussi, H.; Mauro, J. M.; Goldman, E. R.; Anderson, G. P.; Sundar, V. C.; Mikulec, F. V.; Bawendi, M. G. *J Am Chem Soc* **2000**, *122*, 12142.

(52) Medintz, I. L.; Clapp, A. R.; Mattoussi, H.; Goldman, E. R.; Fisher, B.; Mauro, J. M. *Nature Materials* **2003**, *2*, 630.

(53) Clapp, A. R.; Medintz, I. L.; Mauro, J. M.; Fisher, B. R.; Bawendi, M. G.; Mattoussi, H. *J Am Chem Soc* **2004**, *126*, 301.

(54) Dif, A.; Boulmedais, F.; Pinot, M.; Roullier, V.; Baudy-Floc'h, M.; Coquelle, F. M.; Clarke, S.; Neveu, P.; Vignaux, F.; Le Borgne, R.; Dahan, M.; Gueroui, Z.; Marchi-Artzner, V. *J Am Chem Soc* **2009**, *131*, 14738.

(55) Wang, W. T.; Ji, X.; Bin Na, H.; Safi, M.; Smith, A.; Palui, G.; Perez, J. M.; Mattoussi, H. *Langmuir* **2014**, *30*, 6197.

(56) Susumu, K.; Mei, B. C.; Mattoussi, H. *Nature Protocols* **2009**, *4*, 424.

(57) Hens, Z.; Martins, J. C. *Chemistry of Materials* **2013**, *25*, 1211.

(58) Einstein, A. *Ann Phys-Berlin* **1905**, *17*, 549.

(59) Edward, J. T. *J Chem Educ* **1970**, *47*, 261.

(60) Pons, T.; Uyeda, H. T.; Medintz, I. L.; Mattoussi, H. *J Phys Chem B* **2006**, *110*, 20308.

(61) Mattoussi, H.; Cumming, A. W.; Murray, C. B.; Bawendi, M. G.; Ober, R. *Phys Rev B* **1998**, *58*, 7850.

(62) Paiva, T. B.; Tominaga, M.; Paiva, A. C. M. *Journal of Medicinal Chemistry* **1970**, *13*, 689.

(63) Aldeek, F.; Safi, M.; Zhan, N. Q.; Palui, G.; Mattoussi, H. *ACS Nano* **2013**, *7*, 10197.

(64) Medintz, I. L.; Pons, T.; Susumu, K.; Boeneman, K.; Dennis, A. M.; Farrell, D.; Deschamps, J. R.; Melinger, J. S.; Bao, G.; Mattoussi, H. *J Phys Chem C* **2009**, *113*, 18552.

(65) LaVoie, M. J.; Ostaszewski, B. L.; Weihofen, A.; Schlossmacher, M. G.; Selkoe, D. J. *Nat Med* **2005**, *11*, 1214.

(66) Olanow, C. W.; Tatton, W. G. *Annu Rev Neurosci* **1999**, *22*, 123.

(67) Jiang, D.; Shi, S.; Zhang, L.; Liu, L.; Ding, B.; Zhao, B.; Yagnik, G.; Zhou, F. *ACS Chemical Neuroscience* **2013**, *4*, 1305.

(68) Mosca, L.; Lendaro, E.; d'Erme, M.; Marcellini, S.; Moretti, S.; Rosei, M. A. *Neurochemistry International* **2006**, *49*, 262.

(69) Sulzer, D.; Bogulavsky, J.; Larsen, K. E.; Behr, G.; Karatekin, E.; Kleinman, M. H.; Turro, N.; Krantz, D.; Edwards, R. H.; Greene, L. A.; Zecca, L. *Proceedings of the National Academy of Sciences* **2000**, *97*, 11869.

(70) Ji, X.; Palui, G.; Avellini, T.; Na, H. B.; Yi, C.; Knappenberger, K. L.; Mattoussi, H. *J Am Chem Soc* **2012**, *134*, 6006.

(71) Ji, X.; Wang, W.; Mattoussi, H. *Physical Chemistry Chemical Physics* **2015**, *17*, 10108.

(72) Ji, X.; Makarov, N. S.; Wang, W.; Palui, G.; Robel, I.; Mattoussi, H. *The Journal of Physical Chemistry C* **2015**, *119*, 3388.

(73) Low, P. S.; Henne, W. A.; Doorneweerd, D. D. *Accounts of Chemical Research* **2008**, *41*, 120.

(74) Campbell, I. G.; Jones, T. A.; Foulkes, W. D.; Trowsdale, J. *Cancer Research* **1991**, *51*, 5329.

(75) Lee, R. J.; Low, P. S. *Journal of Biological Chemistry* **1994**, *269*, 3198.

(76) Kamen, B. A.; Capdevila, A. *P Natl Acad Sci USA* **1986**, *83*, 5983.

(77) Bharali, D. J.; Lucey, D. W.; Jayakumar, H.; Pudavar, H. E.; Prasad, P. N. *J Am Chem Soc* **2005**, *127*, 11364.

(78) Lu, Y. J.; Low, P. S. *Adv Drug Deliver Rev* **2002**, *54*, 675.

(79) Hermanson, G. T. *Bioconjugate Techniques, 3rd Edition* **2013**, 1.

(80) Wang, W. T.; Aldeek, F.; Ji, X.; Zeng, B. R.; Mattoussi, H. *Faraday Discussions* **2014**, *175*, 137.

Figures and captions

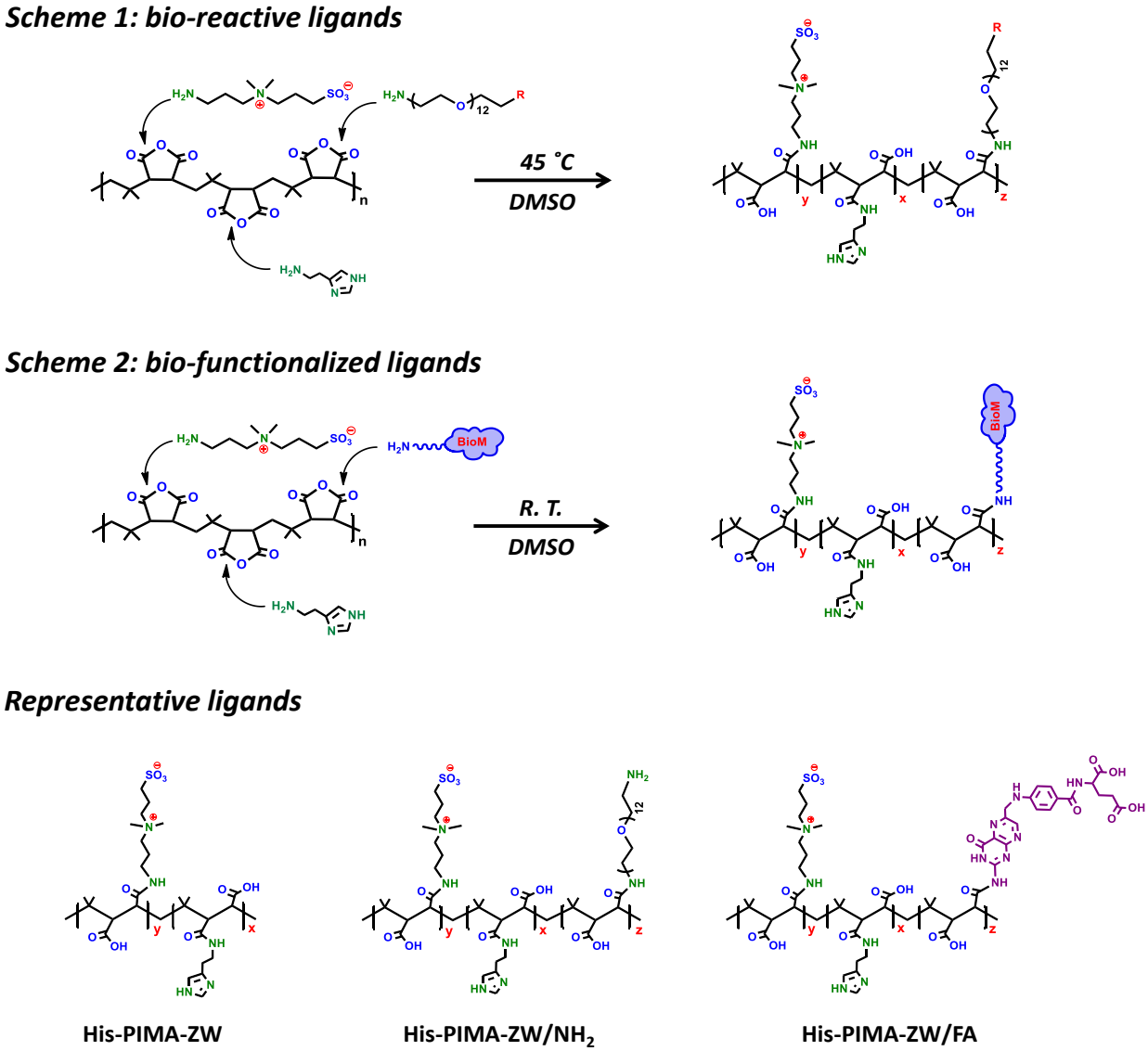

Figure 1. Schematic representation of the ligand synthesis using the one-step nucleophilic addition reaction starting with poly(isobutylene-*alt*-maleic anhydride): bio-reactive ligands (scheme 1) and in-situ bio-functionalized ligands (scheme 2). Structures of three representative ligands are shown in the bottom: His-PIMA-ZW, His-PIMA-ZW/NH_2 and folic acid-modified ligand, His-PIMA-ZW/FA.

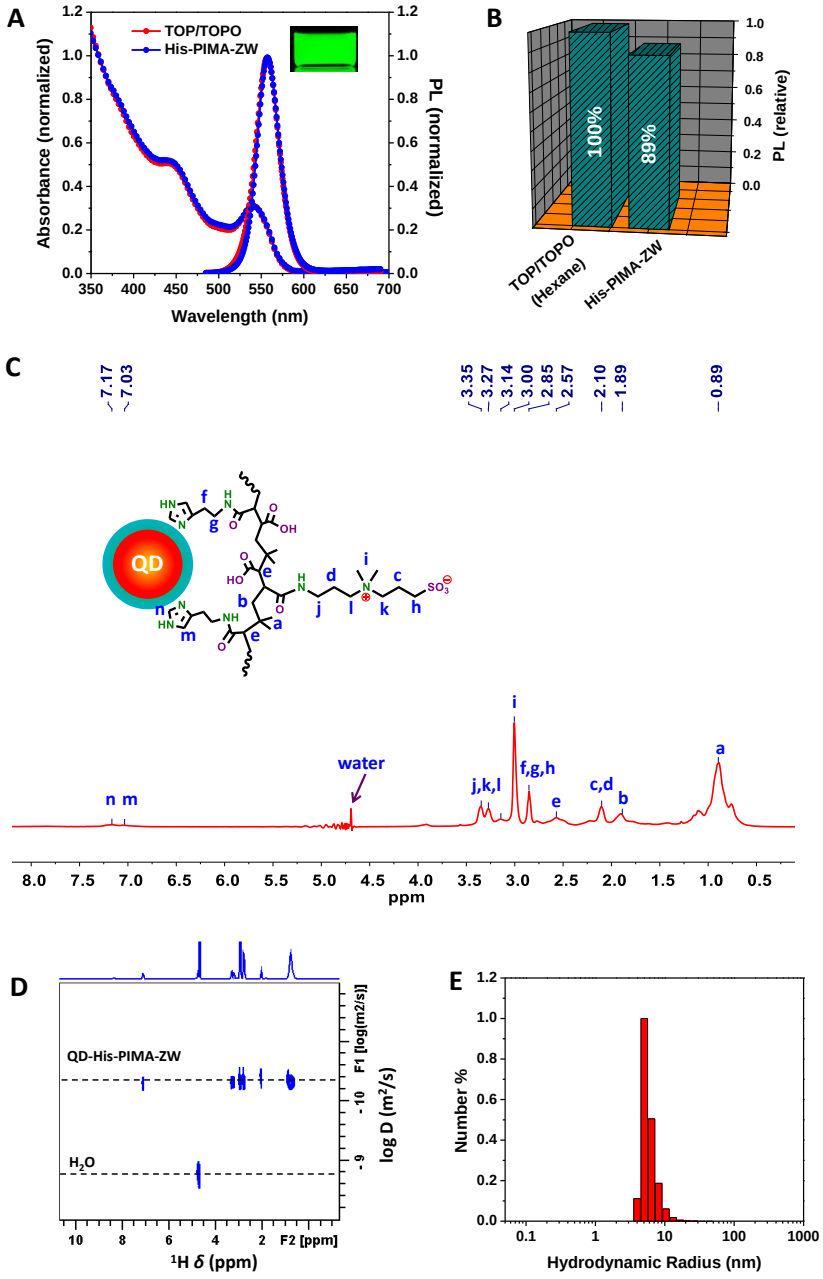

Figure 2. (A) Absorption and emission spectra of QDs (emitting at 556 nm) capped with TOP/TOPO in hexane (red line) and His-PIMA-ZW in H_2O (blue line). Inset shows the fluorescence image of an aqueous QD dispersion (0.5 μM) irradiated using a hand UV lamp (λ_{exc} = 365 nm). (B) PL intensity of His-PIMA-ZW-QDs in buffer (pH 7.5) relative to the intensity measured for the native QDs in hexane; the same optical density is used for both samples. (C) Pulsed-field gradient-based water suppression ^1H NMR spectrum of hydrophilic QDs (in D_2O); assignment of the various peaks is detailed on the ligand structure. (D) DOSY NMR spectrum collected from QDs capped with His-PIMA-ZW in D_2O. (E) Histogram of the hydrodynamic size distribution measured for QDs capped with His-PIMA-ZW extracted from the dynamic light scattering measurement.

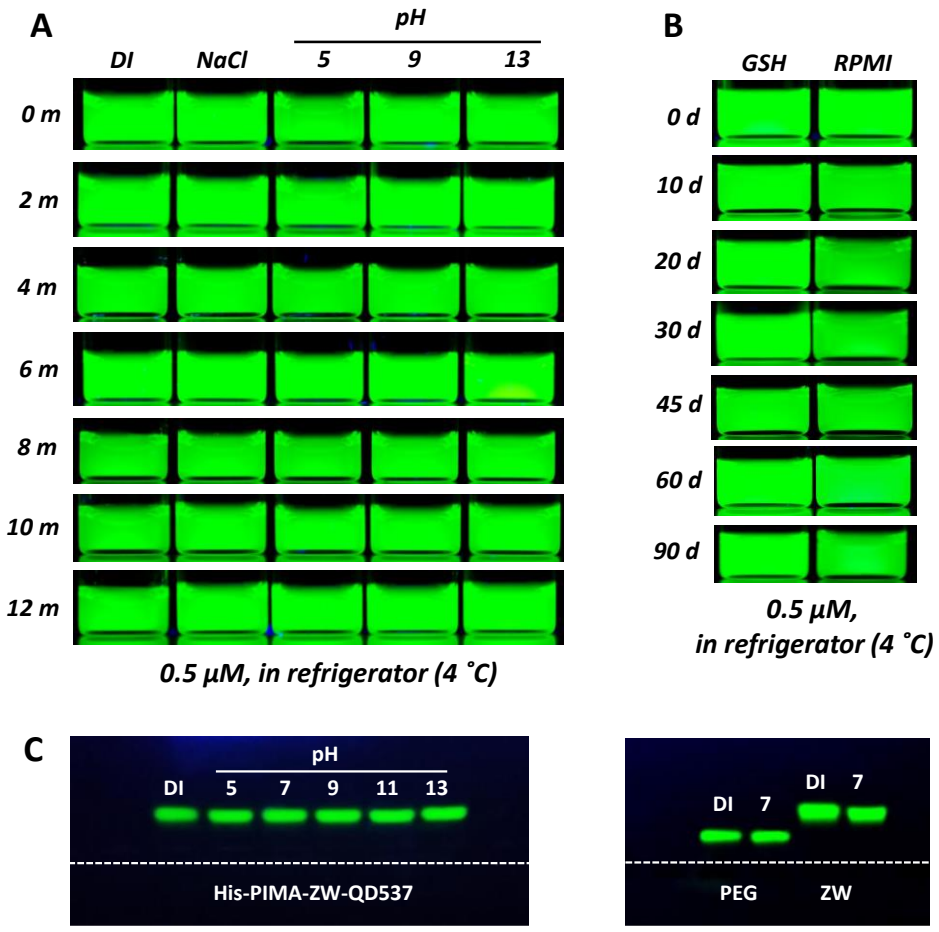

Figure 3. (A) Colloidal stability tests of QDs ligated with His-PIMA-ZW dispersed in DI water, NaCl solution (1 M), and in phosphate buffer (20 mM) with different pH (5 to 13) for 12-month storage. (B) Stability tests (over 3 month-storage) of QD dispersions in the presence of 10 mM glutathione (GSH) and when mixed with growth media (RPMI-1640). The concentration of QDs was ~0.5 μM. All samples were stored at 4 °C. (C) Agarose gel electrophoresis images of QDs ligated with His-PIMA-ZW at different pH from 5 to 13 (left) side-by-side with images of QDs ligated with LA/His-PIMA-PEG (described in reference 39) dispersed in DI water and at pH 7 buffer (right). The concentration of QDs is ~0.5 μM. The dashed line indicates the location of the loading wells.

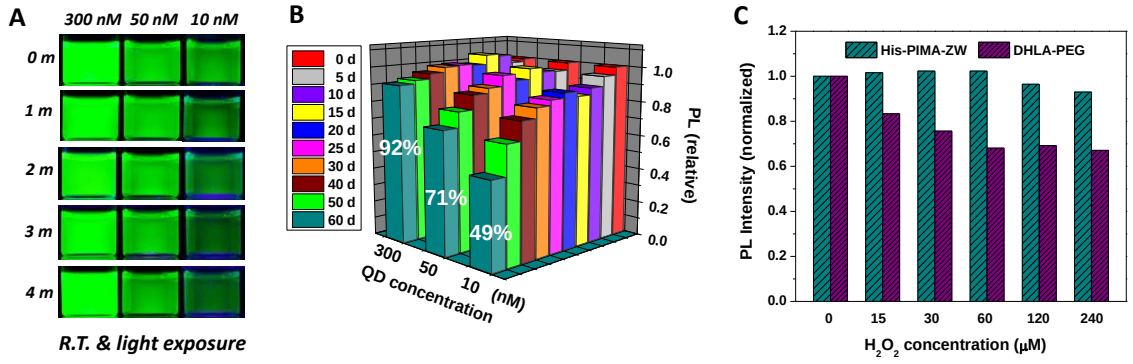

Figure 4. (A) Fluorescence images for three sets of QD dispersions during storage at room temperature and under light exposure for up to 4 months. The concentrations were 300 nM, 50 nM and 10 nM, respectively. (B) Time progression of the PL intensities of these three QD samples normalized with respect to the value measured at day 0. (C) The normalized PL intensities of His-PIMA-ZW-QDs and DHLA-PEG-QDs against chemical oxidation in the presence of increasing concentration of H_2O_2.

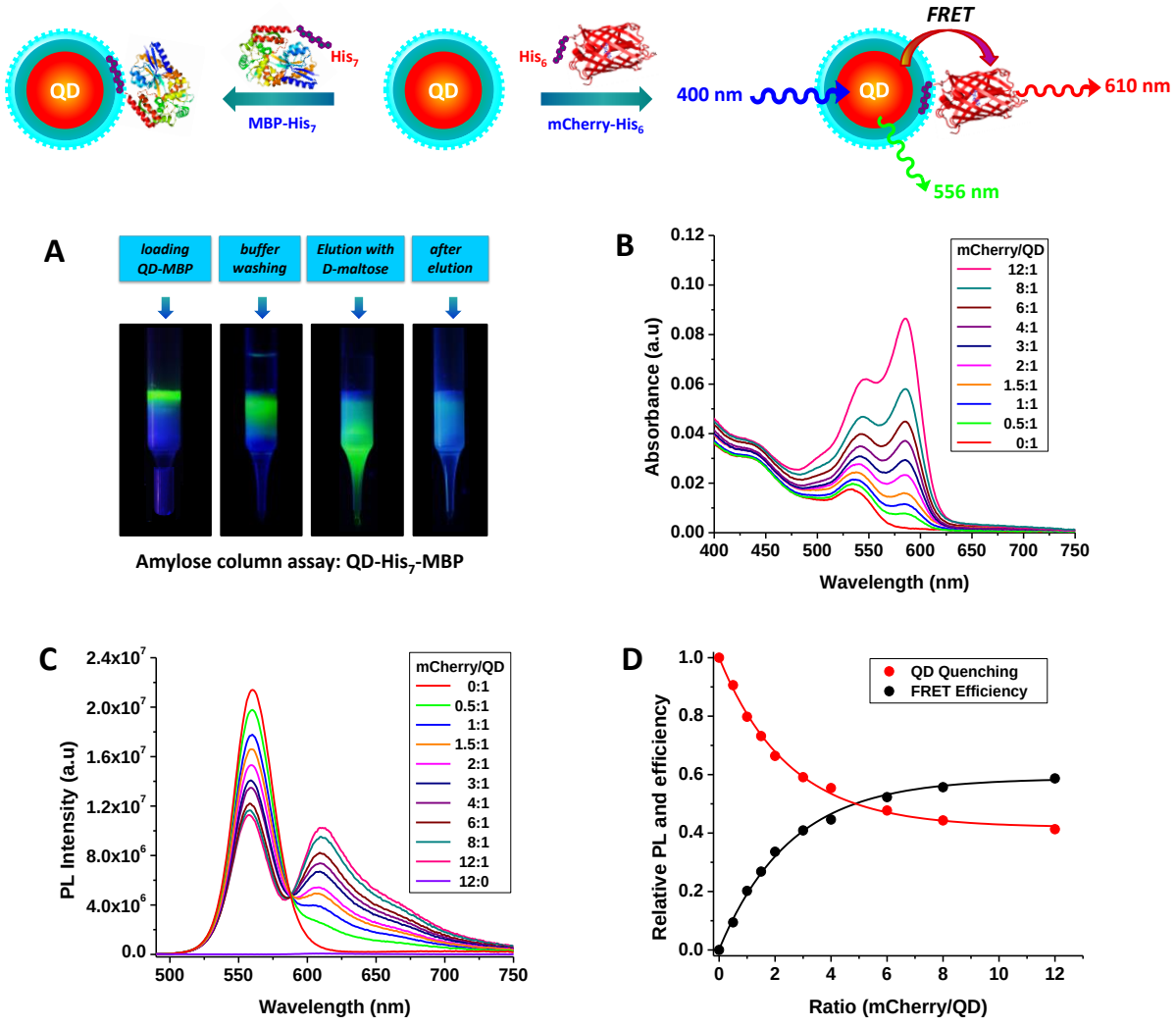

Figure 5. (top) Schematic representation of the bioconjugation between His-PIMA-ZW-QDs and proteins driven by polyhistidine coordination. (A) Amylose chromatography assay testing conjugation of QDs with MBP-His_7; the ratio of MBP to QD was 12:1. (B and C) Evolution of absorption and emission spectra of QD-mCherry-His_6 conjugates as a function of the protein-to-QD ratio (valence) varied between 0:1 and 12:1. (D) Experimental values for the relative QD PL decay (red dot) versus valence *n* together with the corresponding FRET efficiency (black dot) with a fit to hyperbolic function in the form: $E = nR_0^6/(nR_0^6 + r^6)$. Additional details on the FRET analysis is provided in the Supporting Information.

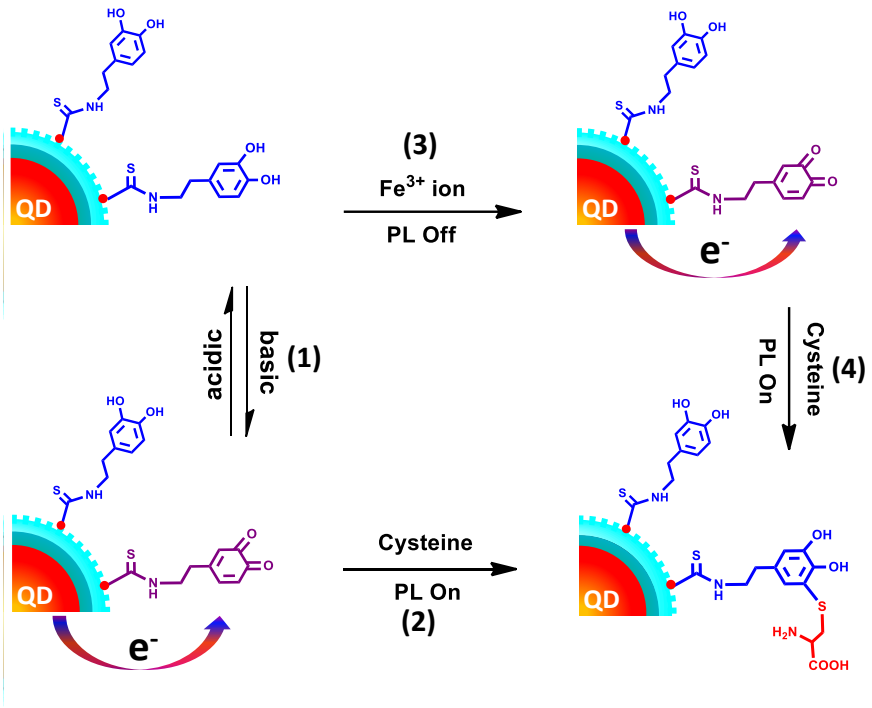

Figure 6. Schematic representation of the changes in the charge transfer interactions between QDs and proximal dopamine as a function of pH, added cysteine or iron ions.

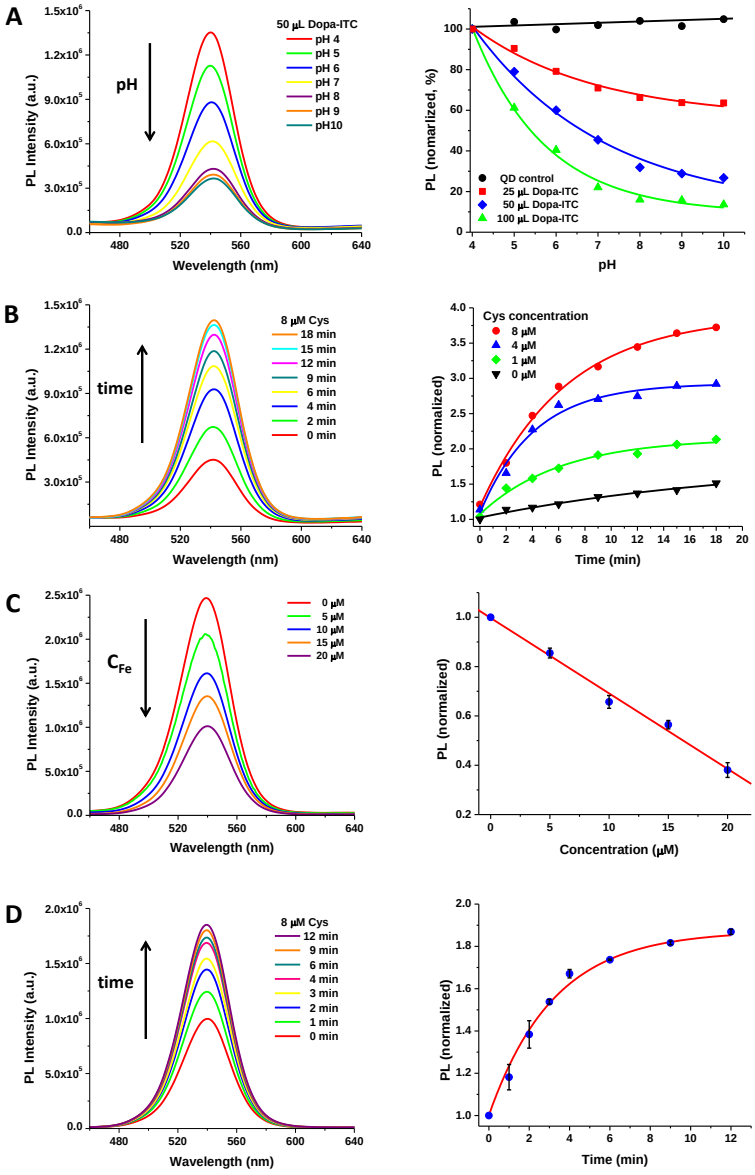

Figure 7. (A) PL spectra collected from dispersions of QD-dopamine conjugates at pH from 4 to 10, together with the integrated PL intensity normalized with respect to the value at pH 4. The PL spectra (left) collected from the conjugates were prepared using 50 µL of dopamine-ITC (see experimental section). (B) Time progression of PL spectra of QD-dopamine conjugates (initially dispersed in pH 10) mixed with 8 µM cysteine. Also shown are plots of the integrated PL progression with time for different concentrations of added cysteine. The PL is normalized with respect to the initial value at 0 min (without cysteine). (C) The PL spectra of QD-dopamine conjugates (prepared using 25 µL of dopamine-ITC) in the presence of different concentrations of Fe from 0 to 20 µM, together with the integrated PL normalized with respect to the value at 0 µM Fe. (D) The time progression of PL spectra of Fe-catalyzed QD-dopamine conjugates in the presence of 8 µM cysteine, together with the relative integrated PL (with respect to the value at 0 min).

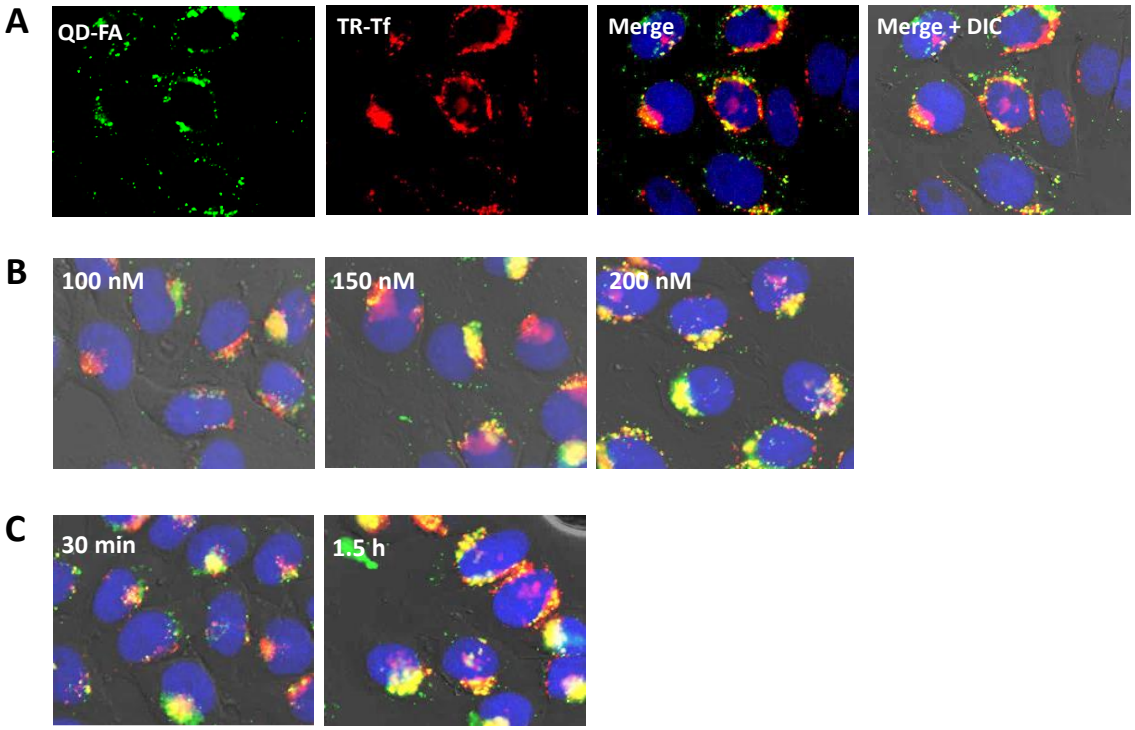

Figure 8. (A) Representative epi-fluorescence images collected from HeLa cells co-incubated with 200 nM QD-FA and 0.5 μM Texas Red-transferrin for 1 hour. The panels correspond to QD fluorescence (green, ~537 nm), Texas Red-transferrin as endosome-specific marker (red, ~615 nm), composite images with DAPI (blue, ~460 nm) and differential interference contrast (DIC) respectively. (B) Concentration-dependent cellular internalization of QD-FA. The merged fluorescent images were collected for HeLa cells co-incubated with 537-nm emitting QD-FA at different concentration: 100 nM (left), 150 nM (middle) and 200 nM (right), along with 0.5 μM Texas Red-transferrin. (C) Time-dependent intracellular uptake of QD-FA. The composite images were collected for HeLa cells co-incubated with 200 nM QD-FA and 0.5 μM Texas Red-transferrin for 30 min and 1.5 hours.

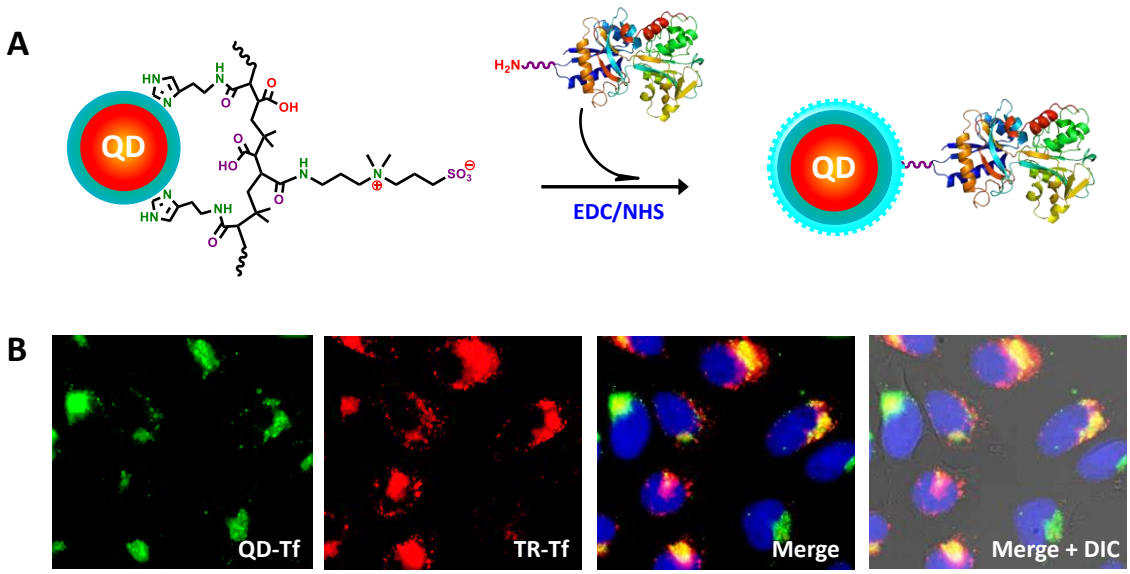

Figure 9. (A) Schematic of the QD-transferrin conjugates assembly via EDC/NHS coupling. (B) Representative images for HeLa cells incubated with 200 nM QD-transferrin conjugates for 1 hour, then with 0.5 µM Texas Red-transferrin for 40 min. The corresponding QD fluorescence (green), Texas Red-transferrin fluorescence (red), composite images with DAPI fluorescence (blue) and differential interference contrast (DIC) are shown.

TOC

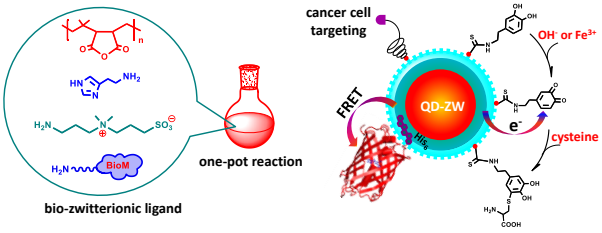
cancer cell targeting
OH⁻ or Fe³⁺
FRET
QD-ZW
e⁻
cysteine
one-pot reaction
bio-zwitterionic ligand